Neutron-scattering study of the dynamical spin susceptibility in $YBa_2Cu_3O_{6.6}$

J. M. Tranquada, P. M. Gehring, and G. Shirane
Brookhaven National Laboratory, Upton, New York 11973

S. Shamoto and M. Sato
Department of Physics, Nagoya University, Nagoya 464-01, Japan
(Received 4 February 1992)

We report a detailed neutron-scattering study of the dynamical spin susceptibility in a single crystal of $YBa_2Cu_3O_{6+x}$, with $x = 0.6$ and $T_c = 53$ K. The measurements cover the energy range from 5 to 50 meV, and temperatures from 10 to 100 K. It is shown that antiferromagnetic correlations between nearest-neighbor CuO_2 layers are quite strong. As a result, only in-phase bilayer spin fluctuations are observed at low energies, with the out-of-phase fluctuations making a weak appearance at 40 meV. Within the two-dimensional (2D) Brillouin zone corresponding to a single layer, the imaginary part of the dynamical susceptibility $\chi''(\mathbf{Q},\omega)$ exhibits a broad peak about the point corresponding to antiferromagnetic order $\mathbf{Q}_{AF}$ with a width that is mildly energy dependent. At 10 K, $\chi''(\mathbf{Q}_{AF},\omega)$ has a rather sharp peak near 27 meV; integrating χ'' over the 2D magnetic Brillouin zone makes the peak in energy much broader. (We have verified that the falloff at high energies also occurs in a previously studied crystal with $x = 0.5$, $T_c = 50$ K.) Although the amplitude at 5 meV and 10 K is near zero, considerable spectral weight is observed at energies well below the weak-coupling limit for 2Δ, where Δ is the superconducting gap. The temperature dependence of the 2D $\mathbf{Q}$-integrated χ'' is well described by a simple function containing a temperature-independent energy gap of 9 meV. A study of the $\mathbf{Q}$ dependence of χ'' at $\hbar\omega = 15$ meV indicates that the signal falls off rather abruptly on moving away from $\mathbf{Q}_{AF}$ (compared to a simple Gaussian distribution). Measurements along two different directions in the 2D zone suggest that the width of the distribution about $\mathbf{Q}_{AF}$ is anisotropic. These results are discussed in the context of current theoretical models.

I. INTRODUCTION

A central issue in the debate over the mechanism of superconductivity in the copper oxides concerns the degree to which electron-electron interactions are responsible for the unusual normal-state properties of these materials.[1] One important manifestation of many-body effects is the existence of spin correlations. For example, in the tetragonal phase of $YBa_2Cu_3O_{6+x}$ the strong Coulomb interaction between Cu $3d$ electrons causes the compound to be an antiferromagnetic insulator.[2] With increasing oxygen content the structure becomes orthorhombic, and charge transfer from the CuO chains dopes holes into the CuO_2 planes.[3,4] The doping destroys the long-range magnetic order[5,6] and makes possible the superconductivity. However, despite the lack of static order, dynamical spin correlations survive[7–9] and provide a measure of the importance of electron-electron interactions in the metallic regime.

Neutron scattering is a unique probe of both the $\mathbf{Q}$ and ω dependence of the imaginary part of the dynamical spin susceptibility χ''. The power of the technique is moderated by the weakness of the scattering, and the resulting requirement of very large single-crystal samples. The nonoperative condition of certain neutron-scattering facilities has also had a dampening effect on research. Happily for us, the restart of the High Flux Beam Reactor (HFBR) at Brookhaven National Laboratory has enabled a redoubled effort to fill in a number of gaps in our knowledge of magnetic correlations in superconducting $YBa_2Cu_3O_{6+x}$.

Over the last several years, nuclear magnetic resonance (NMR) and nuclear quadrupole resonance (NQR) studies have provided valuable information on the zero-frequency limit of the $\mathbf{Q}$-averaged dynamical susceptibility.[10] Comparison of the nuclear relaxation rates measured at Cu and O sites provides strong evidence that the dynamical susceptibility is enhanced in the neighborhood of the wave vector $\mathbf{Q}_{AF}$ corresonding to antiferromagnetic order in the insulating phase. Those results have inspired a significant amount of theoretical work.[11] However, some of the phenomenological models[12,13] that have been developed for the dynamical susceptibility involve parameters that are not uniquely determined by the NMR measurements and contain predictions for finite-frequency behavior that need to be tested. There are a number of questions left to be addressed by neutron scattering. For example, what is the energy scale of the antiferromagnetic spin fluctuations? What is the detailed $\mathbf{Q}$ dependence of the susceptibility near the antiferromagnetic wave vector? Is there a well-defined correlation length? Is there evidence for peaks at incommensurate positions? What are the effects of interlayer coupling?

Together with various collaborators, we have been making piecemeal attacks on these problems.[7,8,14–16] At the same time, a number of intriguing results on

the doping dependence of the spin susceptibility in $YBa_2Cu_3O_{6+x}$ have been reported by Rossat-Mignod and co-workers.[9,17–19] Unfortunately, the latter group has not published sufficient data to substantiate all of their claims, and many details require clarification. We report here on a more comprehensive study of one particular specimen having an oxygen content $x = 0.6$ and a superconducting transition temperature T_c of 53 K. Measurements of **Q**-dependent magnetic scattering at excitation energies from 5 to 50 meV and temperatures from 10 to 100 K are presented. Both the **Q** and ω dependence of χ'' are carefully evaluated, yielding a number of results, which in some cases are in conflict with the work of Rossat-Mignod and co-workers.[17–19] Complications due to phonon scattering and experimental artifacts are also discussed. We believe that contributions from phonons are responsible for some discrepancies between our results and the interpretations of Rossat-Mignod and co-workers.

Our measurements demonstrate that spin fluctuations in nearest-neighbor CuO_2 planes of a superconducting sample have a strong antiferromagnetic correlation over a surprisingly large frequency range. At an excitation energy of 27 meV, only in-phase bilayer fluctuations are observed; out-of-phase fluctuations are still weak, though detectable, at 40 meV. As a result, we have focused on the in-phase modes, which we label "acoustic" in analogy with the lower-energy spin-wave branches observed in antiferromagnetic $YBa_2Cu_3O_{6+x}$.[20,21] Within the two-dimensional (2D) Brillouin zone corresponding to a single CuO_2 layer, the amplitude of the acoustic χ'' is broadly peaked about the antiferromagnetic point $\mathbf{Q}_{AF}$. As a function of frequency, $\chi''(\mathbf{Q}_{AF},\omega)$ measured at 10 K peaks rather sharply near 27 meV. However, because of the linear increase in the Q width with increasing energy, the magnitude of χ'' integrated over the 2D magnetic Brillouin zone exhibits a broad peak near 30 meV. (In contrast, Rossat-Mignod and co-workers[17–19] claim that the Q width is completely energy independent, thus implying that the **Q**-integrated spectral weight falls rapidly at higher energies.) Motivated by these results, we have reexamined a previously studied crystal with $x = 0.5$ and $T_c = 50$ K,[8,15] and verified that its acoustic χ'' also falls off above 30 meV.

As for the temperature dependence, $\chi''(\mathbf{Q}_{AF},\omega)$ at energies between 9 and 30 meV shows a significant increase as T drops from 100 to 10 K. On the other hand, the signal at 5 meV drops toward zero below 50 K. This behavior is consistent with the gaplike frequency dependence at low temperatures previously reported for this crystal.[16] Note that the appearance of a low-temperature spin gap in superconducting $YBa_2Cu_3O_{6+x}$ was discovered by Rossat-Mignod and co-workers.[9,17]

A careful examination of the 2D **Q** dependence of χ'' at fixed frequency also yields interesting results. The 2D **Q** dependence is commonly modeled by either a Lorentzian or Gaussian with an isotropic width. For the present sample, however, a high-resolution scan along the zone diagonal shows a flat-topped peak with steep sides. To check for anisotropy, we have also measured along a path slightly rotated from the zone diagonal. We show that the data are consistent with a structure involving four unresolved Gaussians displaced symmetrically from $\mathbf{Q}_{AF}$ along the [100] and [010] directions. Such a structure is similar in symmetry to that observed in $La_{2-x}Sr_xCuO_4$.[22–24]

The rest of the paper is organized as follows. The next section describes experimental procedures, including the characterization of the crystal. The data are presented and parametrized in Sec. III. In Sec. IV we discuss the significance of our results and compare them with theoretical models. The main body of the paper concludes with a summary in Sec. V. We have also included two appendixes. Appendix A describes an analytic deconvolution of the scattering measurements, assuming a cross section with a Gaussian **Q** dependence. Appendix B explains the occurrence of spurious peaks due to accidental Bragg scattering.

II. EXPERIMENTAL PROCEDURE

The crystal used in this study, originally labeled No. 30, was grown at the Institute for Molecular Science in Japan by a method described in detail elsewhere.[25] It has a large volume, roughly 1 cm^3, and was initially prepared with an oxygen content $x = 0.45$ and $T_c = 45$ K. After several studies,[7,8,14] it was decided to increase the oxygen content of the crystal. Annealing at 650 °C in air for 8.5 days changed x to 0.6. It should be noted that the crystal is actually a mosaic distribution of many small crystals, with a mosaic width of 1.6° as determined by neutron diffraction. Such a structure is advantageous for the homogeneous uptake of oxygen. The room-temperature lattice parameters of the crystal, measured on a calibrated neutron spectrometer, are $a = 3.842$ Å, $b = 3.878$ Å, and $c = 11.738$ Å. A measurement of the ac susceptibility, shown in Fig. 1, indicates a transition to the superconducting state at 53 K. While the ac technique probes only the outer skin of the sample, the relative sharpness of the transition is nevertheless suggestive of homogeneity in the oxygen distribution. The modified crystal is relabeled as No. 30b. We will also present some

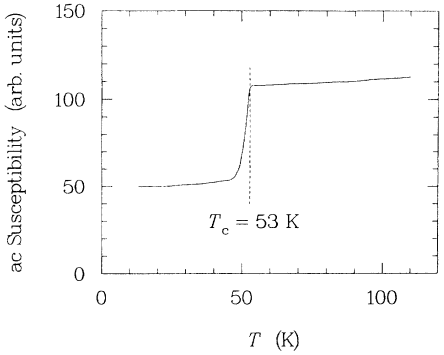

FIG. 1. Temperature dependence of the ac susceptibility measured for crystal No. 30b. The superconducting transition temperature is indicated by the dashed line.

results for crystal No. 29, with $x = 0.5$ and $T_c = 50$ K; it is described in Ref. 7.

For the neutron-scattering measurements, the crystal was oriented with its $[1\bar{1}0]$ axis vertical, so that we could reach any $\mathbf{Q}$ of the form (h, h, l). [We will specify $\mathbf{Q}$ vectors in reciprocal-lattice units (r.l.u.), so that $(1, 1, 1)$ corresponds to $(2\pi/a, 2\pi/a, 2\pi/c)$.] The motivation for this choice of orientation will be explained in the next section. The crystal was mounted in an Al can with He exchange gas and attached to the cold finger of a Displex closed-cycle He refrigerator. Temperatures were monitored with either a Pt resistor or Si diode and were controlled to within one or two degrees Celsius, more than sufficient precision for the present purposes.

The measurements were performed on triple-axis spectrometers H4M and H8 at the HFBR. The (002) reflection of pyrolytic graphite (PG) was used for both the monochromator and analyzer. For all scans, except as noted otherwise, the analyzer was set to detect scattered neutrons with a fixed energy of 30.5 meV. A PG filter was placed after the sample to eliminate higher-order neutrons.

Collimators, with horizontal divergences of 40′-40′-80′-80′, were placed between source and monochromator, monochromator and sample, sample and analyzer, and analyzer and detector, respectively. It was observed that the energy resolution calculated using the nominal collimations was much greater than the observed value. The explanation for this became clear when we noticed that the blade spacings of the collimators before and after the sample were approximately 1 cm, the characteristic dimension of the sample. The effective horizontal divergence was determined by the sample size and the distance from the sample to the far end of each collimator. We estimated the effective collimations, and checked that the energy resolution, as well as $\mathbf{Q}$ resolution of Bragg peak scans (using a reference sample), were well described by these values. For H4M the values 40′-20′-30′-60′ were adopted; for H8 we used 40′-20′-60′-80′. We also estimated the vertical collimations, and checked these values by measuring the vertical resolution for a narrow mosaic Cu crystal. The resulting vertical collimations are 60′-125′-140′-420′ and 60′-75′-190′-420′ for H4M and H8, respectively.

III. DATA AND ANALYSIS

A. Preliminaries

It is not a trivial matter to identify the magnetic scattering in metallic crystals of $YBa_2Cu_3O_{6+x}$. The steeply dispersing spin-wave excitations observed in insulating crystals are strongly damped by hole doping of the CuO_2 planes. As a result, the magnetic cross section is dramatically reduced at low energies, where it is most easily separated from phonons, and the Q width in the plane perpendicular to the antiferromagnetic 2D scattering rod $(\frac{1}{2}, \frac{1}{2}, l)$ is greatly increased. The use of polarized neutrons, which could provide an unambiguous measure of the magnetic scattering, is ruled out by the limited flux available with that technique.

To identify the magnetic scattering, we must rely on its $\mathbf{Q}$ dependence. We make the reasonable assumption that the magnetic cross section for the CuO_2 planes is symmetically distributed about the antiferromagnetic scattering rod. We also assume that the Q width perpendicular to the rod should vary in a systematic fashion with the excitation energy $\hbar\omega$ and that the cross section along the rod should exhibit an inelastic structure factor similar to that observed in antiferromagnetic crystals above the Néel temperature. Thus, we expect any modulation of the intensity along l to be sinusoidal, with a period determined by the c-axis spacing between the pairs of CuO_2 layers. In separating magnetic scattering from scattering due to phonons, we also make use of the fact that the phonon cross section is roughly proportional to Q^2 and that it should increase with temperature according to the Bose factor. However, because of the rather complex crystal structure, the phonons can have strongly $\mathbf{Q}$-dependent structure factors.

Because a modulation along the 2D rod is, in fact, observed, we choose to orient the crystal in the (h, h, l) zone. The standard form of measurement is to fix $\hbar\omega$ and l, and to scan h across the antiferromagnetic rod located at $h = \frac{1}{2}$. Some typical scans are shown in Fig. 2. At each energy one observes a peak centered at $(\frac{1}{2}, \frac{1}{2}, -5.4)$, with a width equal to roughly 30% of the antiferromagnetic

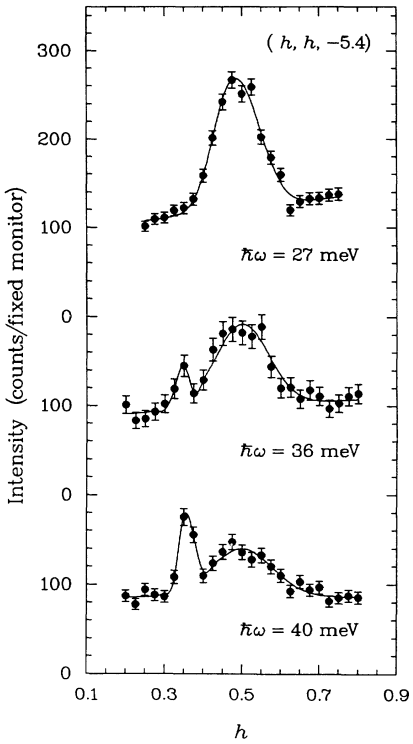

FIG. 2. Scans along $\mathbf{Q} = (h, h, -5.4)$ at $\hbar\omega = 27$, 36, and 40 meV, all measured for the same fixed number of monitor counts at 10 K. The solid lines are fits to the data as discussed in the text. The sharp peaks near $h = 0.35$ are due to accidental Bragg scattering, as explained in Appendix B.

Brillouin zone and an amplitude comparable to the background. The sharp spurious features, especially strong at 40 meV, will be explained shortly.

In order to parametrize the measurements and to correct for resolution effects, we need a model for the $\mathbf{Q}$ and ω dependence of the magnetic cross section. We begin by noting that the scattered intensity is proportional to the scattering function $S_j(\mathbf{Q},\omega)$:

$$I(\mathbf{Q},\omega) \sim \sum_j |F_j(\mathbf{Q})|^2 S_j(\mathbf{Q},\omega), \tag{1}$$

where $F_j(\mathbf{Q})$ is the inelastic structure factor. The index j labels components of the scattering function that correspond to different structure factors. For example, in antiferromagnetic crystals, the coupling between nearest-neighbor CuO_2 planes causes a splitting of the spin waves into acoustic and optical branches, with structure factors given by[20,21]

$$F_{\rm ac}(\mathbf{Q}) = 2f_{\rm Cu}(\mathbf{Q})\sin(\pi zc), \tag{2}$$

$$F_{\rm op}(\mathbf{Q}) = 2f_{\rm Cu}(\mathbf{Q})\cos(\pi zc), \tag{3}$$

where zc is the nearest-neighbor distance between Cu atoms in different planes, and $f_{\rm Cu}(\mathbf{Q})$ is the magnetic form factor for a Cu ion. The acoustic-mode modulation is also observed in metallic $YBa_2Cu_3O_{6+x}$, as we will discuss further in the next subsection.

The scattering function is related to the dynamical spin susceptibility $\chi_j''(\mathbf{Q},\omega)$ by

$$S_j(\mathbf{Q},\omega) = [n(\omega)+1]\,\chi_j''(\mathbf{Q},\omega) \tag{4}$$

$$= \frac{\chi_j''(\mathbf{Q},\omega)}{1-e^{-\hbar\omega/k_BT}}. \tag{5}$$

In selecting a model for χ'' we note that the simple Gaussian fits indicated by the solid lines in Fig. 2 give an adequate characterization of the data. Actually, as will be discussed at the end of this section, the peaks at lower energies are more flat topped, with steeply falling sides, and a pair of incommensurate Gaussians gives a better description. Nevertheless, to give a simple parametrization of the data, we choose to use

$$\chi_j''(\mathbf{Q},\omega) = A_j(\omega)e^{-q^2/2\sigma^2}, \tag{6}$$

where

$$\mathbf{q} = \left(h-\frac{1}{2}, k-\frac{1}{2}, 0\right), \tag{7}$$

and the width σ is allowed to vary with frequency. This model is similar to that used by Hayden *et al.*[26] in their study of $La_{1.95}Ba_{0.05}CuO_4$.

A Gaussian $\mathbf{Q}$ dependence of the cross section is particularly convenient for making corrections for spectrometer resolution. As shown in Appendix A, one can evaluate analytically the convolution of the Gaussian resolution function with the cross section. Hence, the resolution-corrected width $\sigma(\omega)$ and amplitude $A_j(\omega)$ can be extracted easily from simple Gaussian fits to the data. To compare with other work, it is more convenient to specify the half width at half maximum (HWHM), which is related to σ by

$$\text{HWHM} = \sigma\sqrt{2\ln 2}. \tag{8}$$

We now briefly consider the spurious peaks that are observed in Fig. 2. We have found that these features are due to accidental Bragg scattering, as discussed in Appendix B. The peaks are always sharp, their observed positions agree with the calculated ones, and their intensities are essentially temperature independent. In fitting the magnetic scattering, a spurious peak is taken into account by including a second Gaussian in the fit. In fact, there is a spurious contribution to the 27-meV data shown in Fig. 2 that causes the peak to appear displaced away from $h = 0.5$. The size and width of the contamination were determined by a fit to a scan measured at 200 K, where the magnetic signal is considerably reduced.

B. Intensity modulation

In antiferromagnetic $YBa_2Cu_3O_{6+x}$, the optic mode has not been observed in searches up to 60 meV. The persistence of the acoustic-mode intensity modulation at low frequencies in the metallic phase was previously demonstrated in an $x = 0.5$ sample.[14] For the present $x = 0.6$ crystal, we have further characterized the modulation and have found evidence for optic-mode intensity at $\hbar\omega = 40$ meV.

Figure 3 shows a scan along $(\frac{1}{2},\frac{1}{2},l)$ at an excitation energy of 9 meV measured at 100 K. The acoustic modulation is clearly evident. The solid line represents the calculated inelastic structure factor, Eq. (2), with $z = 0.285$ (Refs. 27 and 28) and neglecting the Cu form factor. The calculated curve has been corrected for resolution assuming HWHM= 0.06 Å^{-1} for χ''. While the structure factor is symmetric in l, the intensity is larger at negative l because of a "focusing" effect due to the resolution function, as described in Appendix A. The magnitude of the focusing effect depends on the Q width of χ''—it be-

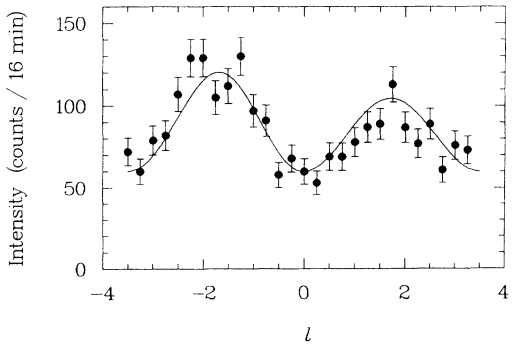

FIG. 3. Scan along $(\frac{1}{2},\frac{1}{2},l)$ measured for an energy transfer of 9 meV at 100 K. For this particular measurement, the incident neutron energy was fixed at 30.5 meV. The solid line is a resolution-corrected calculation of the inelastic structure factor, as discussed in the text, with $z = 0.285$ and HWHM= 0.06 Å^{-1}.

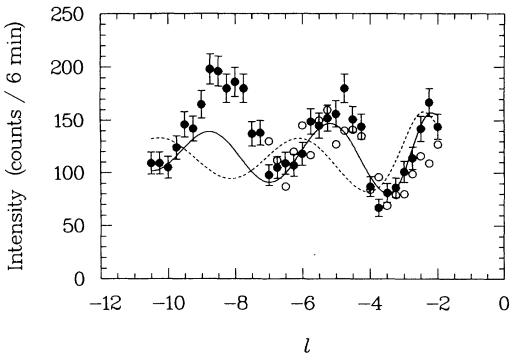

FIG. 4. Scans along $(\frac{1}{2}, \frac{1}{2}, l)$ measured for $\hbar\omega = 27$ meV; solid circles = 10 K and open circles = 100 K. The lines are resolution-corrected calculations of the inelastic structure factor; solid line: $z = 0.285$ and dashed line: $z = 0.244$. For both curves, HWHM= 0.06 Å^{-1}.

comes more pronounced as the width decreases. All of our (h, h, l_0) scans have been performed at negative l_0 values to exploit the focusing effect.

A measurement of the modulation at 27 meV is shown in Fig. 4. Kinematic constraints are responsible for the low-$|l|$ cutoff. The solid line is calculated with the same z and HWHM as used for Fig. 3, although we have also included an additive linear background. The modulation is quite strong at 10 K, but contamination, probably due to phonons, occurs at large $|l|$. (The peak at $l = -4.7$ is due to accidental Bragg scattering, a process discussed in Appendix B.) The decrease in intensity at 100 K corresponds to an overall decrease in the magnetic cross section with increasing temperature. To demonstrate the sensitivity of the modulation to atomic spacing, the dashed line shows the calculated modulation for $z = 0.244$, corresponding to the interlayer spacing between oxygen atoms.[27,28]

The modulation becomes more difficult to test at higher energies because of the decrease in the amplitude of the magnetic scattering. Instead, we have compared (h, h, l_0) scans at values of l_0 corresponding approximately to an acoustic-mode minimum and maximum. Figure 5 shows such measurements at $l_0 = -3.8$ and -5.4 for $\hbar\omega = 40$ meV. From the acoustic-mode structure factor, one would expect a peak intensity ratio for $l_0 = -3.8$ relative to -5.4 of 0.07, whereas the observed ratio is close to 0.5. Hence, it appears that optic-mode intensity starts to show up around 40 meV. To test for the optic mode at higher energies, the scattering kinematics make it necessary to move out to the position of the next optic-mode maximum at $l_0 = -7.1$. Preliminary measurements at that point were inconclusive.

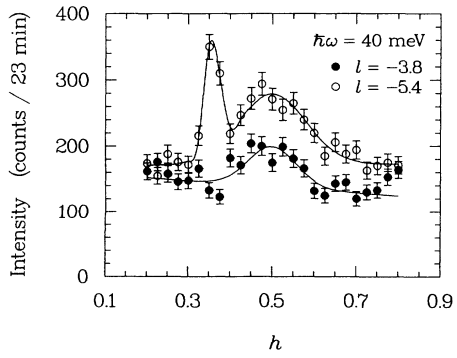

FIG. 5. (h, h, l_0) scans measured at $\hbar\omega = 40$ meV and $T = 10$ K for $l_0 = -3.8$ and -5.4.

C. Frequency dependence

Neutron-scattering measurements,[29] as well as lattice-dynamical calculations,[30,31] have demonstrated that there are numerous weakly dispersing phonon modes in the 12–24-meV energy range. If all of these modes were nondispersive and had **Q**-independent structure factors, then they could simply be treated as a smooth background upon which the magnetic scattering sits, as is apparently assumed by Rossat-Mignod and co-workers.[17–19] Unfortunately, such is not the case.

We have attempted to illustrate the problem in Fig. 6. The solid line shows the scattered intensity as a function of energy measured at $(0.5, 0.5, -5.4)$, the position of the second maximum of the acoustic structure factor. It is necessary to work at this l value in order to achieve energy transfers of $\gtrsim 30$ meV. This 10 K measurement shows a strong peak at approximately 20 meV. Similar data have been reported by Rossat-Mignod and co-workers.[17] The dashed line is an average of measurements at $(0.3, 0.3, -5.4)$ and $(0.7, 0.7, -5.4)$, where we assume the magnetic scattering to be negligible. A much weaker peak, due to phonons, occurs at about 18 meV. If the phonons did not change with h, then one could attribute the difference between the two curves to magnetic scattering. However, the dot-dashed line represents a measurement at $(0.5, 0.5, -5.4)$ and $T = 300$ K, corrected approximately for the Bose factor. Taking the difference between the 300-K data and the low-temperature background measurement would yield a sharp steplike feature

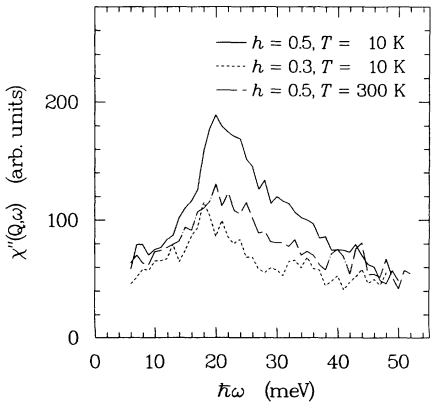

FIG. 6. Constant-**Q** scans at $\mathbf{Q} = (h, h, -5.4)$, corrected for the Bose factor, $1/[1 - \exp(-\hbar\omega/k_B T)]$. Solid line: $h = 0.5$, $T = 10$ K; dashed line: $h = 0.3$, $T = 10$ K; dot-dashed line: $h = 0.5$, $T = 300$ K.

near 20 meV. Such a result is inconsistent with the results that will be presented below. We attribute the anomalous shape of such a difference spectrum to the effects of phonon dispersion and **Q**-dependent phonon structure factors.

Fortunately, the phonon contribution is substantially smaller in the region of $(0.5, 0.5, -1.8)$, and energies up to approximately 27 meV can be studied there. We have performed a series of (h, h, l_0) scans for a wide range of energies, and the data have been parametrized using Eq. (6). To compare measurements at different l_0, we correct for resolution and for the inelastic structure factor (excluding the magnetic form factor). The results for the amplitude, which we denote by $\chi''_{\rm ac}(\mathbf{Q}_{\rm AF}, \omega)$, and the HWHM are presented in Figs. 7 and 8, corresponding to measurements at 10 K and 100 K, respectively.

Looking first at the 10-K results in Fig. 7, we note that the amplitude peaks rather sharply near 27 meV, falling off rapidly at large $\hbar\omega$. At the low-energy end, there is a large jump between 5 and 9 meV. The HWHM shows a roughly linear increase with increasing energy. Systematic errors become more substantial at the higher energies, due to the presence of accidental-Bragg-scattering peaks (see Fig. 2) and the smaller signal-to-background ratio; nevertheless, the resolution generally does not limit the width measurement. We believe that the energy dependence of the width is real, in disagreement with a claim of energy-independence made by Rossat-Mignod and co-workers.[17–19]

At 100 K, we see from Fig. 8 that the low-energy step

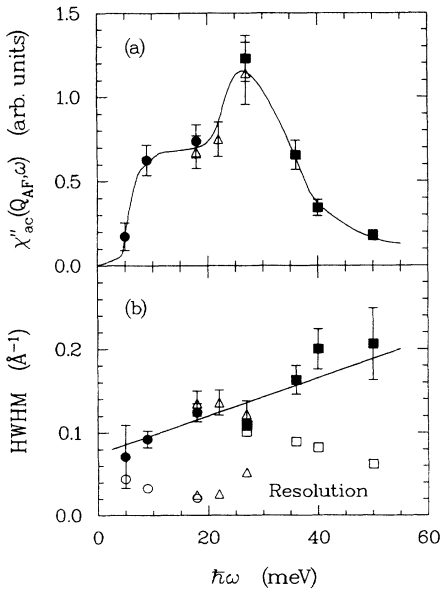

FIG. 7. Resolution-corrected results of Gaussian fits to constant-ω scans measured along (h, h, l_0) at 10 K; circles: $l_0 = -1.8$, triangles: $l_0 = -2.2$, squares: $l_0 = -5.4$. (a) Amplitude of $\chi''(\mathbf{Q}, \omega)$ at $\mathbf{Q} = (\frac{1}{2}, \frac{1}{2}, l_0)$. (b) Half width at half maximum. Open symbols correspond to the effective resolution width when the **Q**-width of $\chi''(\mathbf{Q}, \omega)$ goes to zero. Lines are guides to the eye.

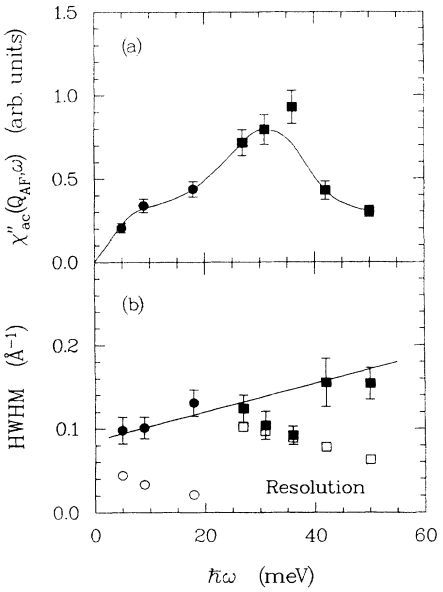

FIG. 8. Resolution-corrected results of Gaussian fits to constant-ω scans, as in Fig. 7, for measurements at 100 K. Lines are guides to the eye.

in the amplitude has disappeared, and there is a significant decrease in the amplitude at energies $\lesssim 30$ meV. At higher energies there is much less change with temperature. The HWHM still varies linearly with $\hbar\omega$, but the slope is smaller than at 10 K. Considering the systematic difficulties in extracting the magnetic cross section at high energies, further work is required to determine whether the change in width with temperature is a real effect. Nevertheless, the lack of any substantial change in width at low energies appears to be real.

To compare with other systems, it is also of interest to consider the **Q**-integrated susceptibility. Since we have an incomplete characterization of the optic-mode contribution at higher energies, we will focus on the 2D **Q** integral of the acoustic part of the dynamical susceptibility. From Eq. (6) we obtain

$$\tilde{\chi}''_{\rm ac}(\omega) = \int d\mathbf{Q}^{\rm 2D} \chi''_{\rm ac}(\mathbf{Q}, \omega) \tag{9}$$

$$= 2\pi\sigma^2 A_{\rm ac}. \tag{10}$$

This quantity is plotted in Fig. 9. One observes that, at 10 K, $\tilde{\chi}''(\omega)$ has a broad peak near 30 meV. At low energy it decreases toward zero near 5 meV, consistent with our previous study.[16] At 100 K, the peak decreases and appears to flatten out. The integrated susceptibility shows a linear variation with frequency at low energy.

Figure 10 shows the temperature dependence of the **Q**-integrated susceptibility at 5, 9, and 18 meV. At 18 meV, $\tilde{\chi}''(\omega)$ increases monotonically with decreasing temperature, whereas at 5 meV there is a large decrease below 50 K. The temperature dependence of the 9 meV data is roughly an average of that at the lower and higher energies.

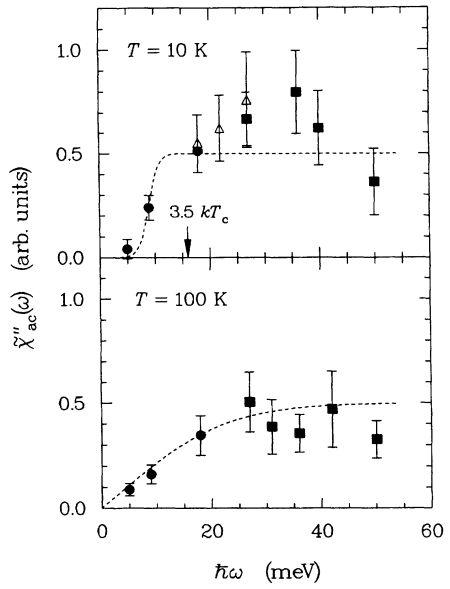

FIG. 9. Two-dimensional-$\mathbf{Q}$ integral of $\chi''_{ac}(\mathbf{Q},\omega)$ calculated from results of Gaussian fits to measurements at 10 K (top) and 100 K (bottom). The dashed lines are model calculations, as described in the discussion section.

The shape of $\chi''_{ac}(\mathbf{Q}_{AF},\omega)$ was previously studied[8,15] for the $x = 0.5$, $T_c = 50$ K crystal. At low temperature (10 K) the signal peaked at $\hbar\omega \approx 30$ meV; however, whether it saturated at that level or decreased at higher energies was unclear. Motivated by the present results for the $x = 0.6$ crystal, we have reexamined the $x = 0.5$ sample. Measurements up to 36 meV are consistent with the earlier work. The situation at higher energies is illustrated in Fig. 11. From a comparison of the $(h,h,-5.4)$ scans at 30 and 43 meV, it is clear that the amplitude of the peak in χ'' decreases rapidly above 30 meV, just as it does for the $x = 0.6$ sample.

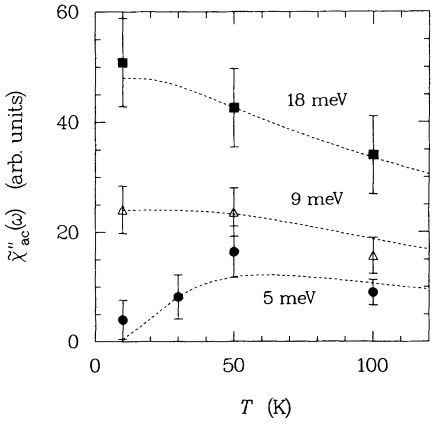

FIG. 10. Temperature dependence of $\tilde{\chi}''(\omega)$ for $\hbar\omega = 5$ meV (circles), 9 meV (triangles), and 18 meV (squares). Dashed lines are model calculations, as described in the discussion section.

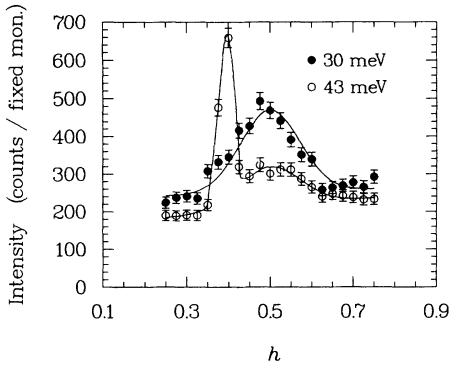

FIG. 11. Scans along $(h,h,-5.4)$ at $\hbar\omega = 30$ meV (solid circles) and 43 meV (open circles) measured at $T = 10$ K for the $x = 0.5$ crystal (No. 29). The lines are fitted curves. The sharp peak at $h = 0.4$ for $\hbar\omega = 43$ meV is due to accidental Bragg scattering.

D. Q dependence

We will now reconsider the question of the $\mathbf{Q}$ dependence of $\chi''(\mathbf{Q},\omega)$. Figure 12(a) shows a scan along $(h,h,-1.8)$ at $\hbar\omega = 15$ meV and $T = 10$ K. The sides of the peak are rather steep and the top is quite flat. Rather than using a single Gaussian to characterize the peak, a much better fit is obtained using a pair of identical Gaussians displaced symmetrically from $h = 0.5$. The solid line corresponds to such a fit, yielding a resolution-corrected HWHM of 0.073 Å^{-1} and a peak separation of 0.156 Å^{-1}. The effective resolution HWHM along the direction of the scan is only 0.025 Å^{-1}.

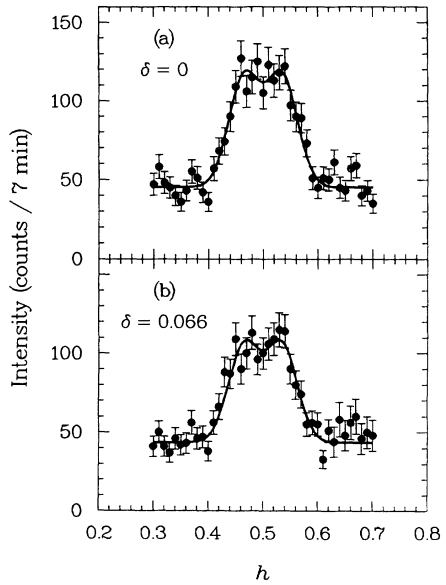

FIG. 12. Scans along $(h(1+\delta),h(1-\delta),-1.8)$ for $\hbar\omega = 15$ meV and $T = 10$ K, measured with the analyzer fixed at 14.7 meV. (a) $\delta = 0$, standard zone-diagonal scan; (b) $\delta = 0.066$, [110] axis tilted by 3.8° out of the scattering plane. Solid lines are fits to the data as discussed in the text.

Although we cannot resolve two peaks in Fig. 12(a), the shape is suggestive of incommensurate structure, as has been observed in $La_{2-x}Sr_xCuO_4$.[22–24] To test this possibility, it is of interest to perform scans along other directions in the 2D plane perpendicular to [001]. The two commonly discussed incommensurate structures each consist of four peaks positioned either at $\left(\frac{1}{2}(1\pm\delta),\frac{1}{2}(1\pm\delta),l_0\right)$ or at $\left(\frac{1}{2}(1\pm\delta),\frac{1}{2},l_0\right)$ and $\left(\frac{1}{2},\frac{1}{2}(1\pm\delta),l_0\right)$, as illustrated in Fig. 13. The two-peak fit suggests $\delta = 0.068$. To test for a diamond-shaped incommensurate structure, the [110] axis in the horizontal plane was tilted vertically by 3.8°. This tilt allowed a scan along the path $\left(h(1+\delta),h(1-\delta),-1.8\right)$ with $\delta = 0.066$; the data collected at 15 meV are shown in Fig. 12(b). The solid line corresponds to a curve calculated with the same peak widths and separation as in (a); the fitted amplitude of (b) is $(88\pm8)\%$ of (a).

To interpret these results, we must take into account the vertical resolution of the spectrometer. Keep in mind that the 2D-zone diagonal lies in, or, in the tilted case, nearly in, the horizontal scattering plane. The orthogonal direction in the 2D plane corresponds to vertical. The vertical-Q resolution is generally much broader than the in-plane resolution. For the experimental conditions used, the vertical (Gaussian) resolution width $(1/\sqrt{M_{33}})$ is 0.064 Å^{-1} (0.039 r.l.u.). Assuming four incommensurate peaks of the second type, each with an isotropic Gaussian width of 0.032 r.l.u., corresponding to the width determined by the fits to the data of Fig. 12, we calculate, using Eq. (A8) and $\delta = \sqrt{2}\times 0.068$, that the measured peak intensity in scan (b) should be 89% of scan (a), in excellent agreement with the observed intensity ratio.

Thus, the data are consistent with four unresolved incommensurate peaks located at $\left(\frac{1}{2}(1\pm\delta),\frac{1}{2},l\right)$ and $\left(\frac{1}{2},\frac{1}{2}(1\pm\delta),l\right)$, with $\delta = 0.096$. The fact that separate peaks are not resolved is due to the cross section itself, and not due to the spectrometer resolution; hence, it may be slightly misleading to use the word incommensurate. Nevertheless, it is interesting to note that the peak position parameter δ obtained here, for a sample with a T_c of 53 K, is less than half the value reported in a recent study of $La_{1.86}Sr_{0.14}CuO_4$, where an incommensurate structure is clearly present but T_c is only 33 K.[24] Considering the correlation between T_c and carrier density,[32] an extrapolation of the monotonic increase of δ with doping observed in $La_{2-x}Sr_xCuO_4$ (Refs. 22–24) would lead one to expect a much greater value for $YBa_2Cu_3O_{6.6}$.

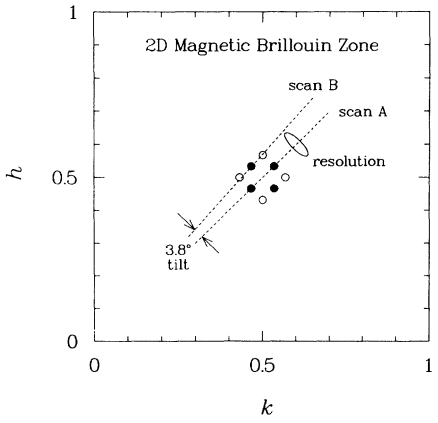

FIG. 13. Diagram of the 2D reciprocal space for a single CuO_2 plane, indicating the paths of the scans shown in Fig. 12. Solid and open circles mark possible alternative locations of incommensurate peaks. Ellipse indicates the half-intensity surface of the resolution function.

IV. DISCUSSION

In this section we discuss the significance of our results, and their relationship to other work. We begin by describing the implications of the observed intensity modulation along $(\frac{1}{2},\frac{1}{2},l)$. Next, the neutron results are compared with NMR studies of the spin susceptibility. After that, we attempt to relate our findings to some theoretical models; in particular, we consider Fermi-liquid-type calculations of the normal-state susceptibility, and various predictions for χ'' in the superconducting state.

A. Implications of the intensity modulation

The intensity modulation along the [001] direction tells us that the spins in nearest-neighbor CuO_2 layers are antiparallel and fluctuate in phase. In the antiferromagnetic, tetragonal phase of $YBa_2Cu_3O_{6+x}$, the modulation results from an exchange coupling $J_\perp$ between layers, which splits the single-layer spin-wave modes into acoustic and optic branches.[20,21] The splitting between branches is proportional to $\sqrt{J_\perp J_\parallel}$, and since the in-plane superexchange $J_\parallel$ is on the order of 100 meV, an interlayer coupling of a few meV can lead to a substantial optic-mode gap. The inelastic structure factors for the two modes are given by Eqs. (2) and (3). In searches up to $\sim$ 60 meV in antiferromagnetic crystals, the optic mode has not yet been observed.

Let us consider for a moment a model in which doping the CuO_2 planes with holes does not modify the magnetic moments on the Cu ions but merely disorders them. The enhancement of the net interlayer coupling by $\sqrt{J_\parallel}$ in the Néel state is the result of long 2D correlation lengths. One would expect that as the range of dynamical correlations is reduced, the net interlayer coupling would correspondingly decrease, eventually reaching a limit of $J_\perp$. It is difficult to make a reasonable theoretical estimate of $J_\perp$. If it is due primarily to direct exchange between Cu $3d$ states, then it would most likely be enhanced by an admixture of $d_{3z^2-r^2}$ holes, for which some evidence exists in related compounds.[33] Nevertheless, it would be surprising if $J_\perp$ is as large as 10 meV, and even then it would be small compared to the kinetic energy of the doped holes. If the doped holes in different planes move independently, then one would expect all interlayer correlations to be completely destroyed. The observation of the acoustic-mode modulation suggests that holes must move coherently in the two planes of a bilayer. Note that

the modulation remains strong both above and below T_c (see Fig. 4); thus, there is no significant change in coherence due to the onset of superconductivity.

This conclusion is also supported by going to the opposite limit and calculating the spin susceptibility for noninteracting electrons. For simplicity, we will consider a model with a single band per layer. With a hopping matrix element t between Cu sites, the energy dispersion of a single band is given by

$$\varepsilon_{\mathbf{k}} = -2t(\cos k_x a + \cos k_y a). \tag{11}$$

Let the interlayer hopping between neighboring Cu sites be $t_\perp$; then the Hamiltonian matrix for the energy bands of a bilayer is

$$H = \begin{pmatrix} \varepsilon_{\mathbf{k}} & t_\perp e^{-ik_z zc} \\ t_\perp e^{ik_z zc} & \varepsilon_{\mathbf{k}} \end{pmatrix}. \tag{12}$$

The eigenvalues are

$$\varepsilon_{\mathbf{k},\pm} = \varepsilon_{\mathbf{k}} \pm t_\perp, \tag{13}$$

and the eigenvectors are

$$|\mathbf{k},\pm\rangle = \frac{1}{\sqrt{2}} \begin{pmatrix} \pm e^{-ik_z zc} \\ 1 \end{pmatrix}. \tag{14}$$

The Lindhard susceptibility is given by[34]

$$\chi(\mathbf{Q},\omega) = \frac{1}{N} \sum_{\substack{\mathbf{k} \\ m,m'}} \frac{f(\varepsilon_{\mathbf{k},m}) - f(\varepsilon_{\mathbf{k}+\mathbf{q},m'})}{\omega - (\varepsilon_{\mathbf{k},m} - \varepsilon_{\mathbf{k}+\mathbf{q},m'}) + i\eta} \times |\langle \mathbf{k}, m | \mathbf{k}+\mathbf{Q}, m' \rangle|^2, \tag{15}$$

where N is the number of sites, and $f(\varepsilon)$, the Fermi distribution function, has the form

$$f(\varepsilon) = \frac{1}{e^{(\varepsilon-\mu)/k_B T} + 1}. \tag{16}$$

Making use of Eq. (14) to evaluate the matrix elements in Eq. (15) yields

$$\chi''(\mathbf{Q},\omega) = (\chi''_{+,-} + \chi''_{-,+}) \sin^2(\pi z l) + (\chi''_{+,+} + \chi''_{-,-}) \cos^2(\pi z l), \tag{17}$$

where

$$\chi''_{m,m'}(\mathbf{Q},\omega) = \pi \sum_{\mathbf{k}} [f(\varepsilon_{\mathbf{k},m}) - f(\varepsilon_{\mathbf{k}+\mathbf{Q},m'})] \times \delta(\omega + \varepsilon_{\mathbf{k},m} - \varepsilon_{\mathbf{k}+\mathbf{Q},m'}). \tag{18}$$

In this noninteracting-electron picture, the $\sin^2(\pi z l)$ modulation that we observe is associated with interband scattering of electrons. The fact that we see the modulation indicates that interband and intraband contributions have significantly different ω and/or $\mathbf{q}$ dependences.

Whichever way one chooses to analyze it, the presence of the modulation clearly indicates that the electronic coupling between nearest-neighbor planes is quite strong on an energy scale relevant for the superconductivity. It is interesting to note that Rice *et al.*[35] have found evidence for a strong coupling of the superconductivity within CuO_2 bilayers from transport measurements on a single crystal of $YBa_2Cu_3O_{7-x}$. The relationship between the bilayer spin correlations and superconductivity remains to be seen.

B. Comparison with NMR and NQR results

Measurements by NMR and NQR of nuclear spin-lattice relaxation rates for ^{63}Cu, ^{17}O, and ^{89}Y nuclei have provided valuable information about the low-frequency limit of χ''.[10] One of the key observations is that the relaxation rate $1/T_1$ is much larger for Cu than for O, even in $YBa_2Cu_3O_7$. The commonly accepted explanation for this behavior involves a strong enhancement of χ'' around $\mathbf{Q}_{AF}$, in qualitative agreement with neutron scattering studies.

Detailed parametrizations of relaxation-rate measurements have been performed by Millis, Monien, and Pines[12] for $YBa_2Cu_3O_7$, and by Monien, Pines, and Takigawa[13] for $YBa_2Cu_3O_{6.63}$ (T_c = 60 K), in terms of an antiferromagnetic-Fermi-liquid (AFL) model. In that model, the $\mathbf{Q}$ dependence of χ'' about $\mathbf{Q}_{AF}$ is assumed to have a squared-Lorentzian form, with a half width (at $\omega = 0$) equal to the inverse of the correlation length ξ. Fitting the $x = 0.63$ data required a correlation length approaching $4a$ at low temperature.[13] There has been some concern over quantitative consistency with the neutron scattering results, because in early studies of an $x = 0.5$ crystal[8,14] we reported $\xi \sim 2a$. From the analysis of the $x = 0.6$ crystal in this paper, we have found that the 2D Q width of the Gaussian peak in χ'' is ω dependent, so that a straightforward determination of the correlation length has not been possible. Nevertheless, taking the inverse of the HWHM at low frequency gives an effective ξ of roughly $3a$, consistent with the results of Rossat-Mignod *et al.*[17] A more important result, however, is that the peak in χ'' falls off much faster than a Lorentzian $\mathbf{Q}$ dependence. We have parametrized the data using a Gaussian, but the scans in Fig. 12 indicate an even sharper $\mathbf{Q}$ dependence. The shape of χ'' is important for the NMR analysis because the relaxation rate measures an average of $\chi''(\mathbf{Q},\omega_0)$ over the Brillouin zone, weighted by a form factor that differs for the Cu and O sites. The sharply defined peak that we observe with neutrons should be more than sufficient to explain the relaxation rate enhancement found for Cu.

To model the temperature dependence of the relaxation rates, the correlation length of the AFL model was assumed to have a substantial temperature dependence.[12,13] While we made a similar assumption in our initial analysis for the $x = 0.5$ sample,[8,14] more recent work has demonstrated that the Q width of the susceptibility peak is essentially temperature independent.[15,17] While we have only studied a restricted temperature range in the present work, the results are consistent with a lack of any susbstantial temperature dependence for the Q width, at least at low energies. (Of course, the lowest energy measured with neutrons is several orders of magnitude greater than that probed by NMR.) In the next subsection, we will discuss other models for the temperature dependence of χ''.

One last point concerns the frequency dependence of the susceptibility. While relaxation rate measurements provide no direct information on this issue, the AFL model assumes a frequency dependence whose parameters are determined by fits to the NMR and NQR data. For the $x = 0.63$ sample at low temperature, the parametrization gives a peak in χ'' at an energy of 3 meV.[13] The direct measurement by neutron scattering for our $x = 0.6$ sample shows that the peak actually occurs at an energy one order of magnitude larger. Note that our result is not in conflict with the NMR and NQR data, but rather with the AFL parametrization.

C. Fermi-liquid models for the susceptibility

The antiferromagnetic Fermi-liquid theory[12] mentioned above is a completely phenomenological model. Other workers[36–40] using a Fermi-liquid approach have started from a particular model for the band structure; they then calculate the Lindhard susceptibility and correct for many-body effects using the random-phase approximation (RPA). The calculations differ according to whether a single-band model[36,37,40] or more realistic dispersion[38,39] is used, and whether the antiferromagnetic exchange (or Coulomb interaction) used in the RPA calculation is a constant[36,37,40] or $\mathbf{Q}$ dependent.[38,39] All calculations involve a single 2D layer, and hence none can describe the coupled bilayer effects that we observe.

Bulut and Scalapino[37] pointed out an interesting feature of the noninteracting system. They considered the case of a single band with the dispersion of Eq. (11), and hole doping, so that $-\mu = |\mu|$. Then for $\mathbf{Q} = \mathbf{Q}_{\rm AF}$, Eq. (18) becomes

$$\chi''(\mathbf{Q}_{\rm AF},\omega) = \frac{\pi}{2}N(\omega/2)[\, f(|\mu| - \hbar\omega/2) - f(|\mu| + \hbar\omega/2)], \tag{19}$$

where $N(\omega)$ is the band density of states. Equation (19) can be rewritten in the form

$$\chi''(\mathbf{Q}_{\rm AF},\omega) = \frac{\pi}{4}N(\omega/2)\left[\tanh\left(\frac{\hbar\omega - 2|\mu|}{4k_BT}\right) + \tanh\left(\frac{\hbar\omega + 2|\mu|}{4k_BT}\right)\right]. \tag{20}$$

Note that for $\mu = 0$ one obtains the factor $\tanh(\hbar\omega/4k_BT)$ derived by Virosztek and Ruvalds[41] for the (perfectly) nested Fermi liquid. [That $\tilde{\chi}''(\omega)$ has such a simple functional dependence on ω/T was postulated by Varma *et al.*[42]] Bulut and Scalapino observed that at low temperatures, χ'' is suppressed for $\hbar\omega \lesssim 2|\mu|$. Thus, at $\mathbf{Q}_{\rm AF}$ a pseudogap structure would appear as the temperature is lowered.

The reason that the gap appears is that for finite μ, $\mathbf{Q}_{\rm AF}$ no longer spans the Fermi surface, and hence the occurrence of spectral weight at that point depends on thermal smearing. On the other hand, even at low temperature, χ'' has peaks at incommensurate wave vectors $\mathbf{Q}^*$, which are displaced from $\mathbf{Q}_{\rm AF}$ along the [100] and [010] directions.[37] Thus, for the noninteracting-electron system the gaplike behavior appears only near $\mathbf{Q}_{\rm AF}$, while incommensurate peaks remain strong.

The gaplike behavior that we observe for the $x = 0.6$ crystal occurs for the entire Q width of the peak in χ''. If incommensurate structure is present, it does not appear to be resolvable. Even at the lowest energies, the vertical resolution is sufficiently coarse that significant incommensurate structure has not escaped measurement. Hence, the simple picture given by Bulut and Scalapino[37] to explain the pseudogap observed in neutron-scattering measurements[17,16] is inadequate. Nevertheless, it suggests an interesting functional form for comparison with the data. Without concern for theoretical justification, we have found that several features of the temperature and energy dependence of the $\mathbf{Q}$-integrated susceptibility are well described by the formula

$$\tilde{\chi}''(\omega) = A\left[\tanh\left(\frac{\hbar(\omega - \omega_g)}{2k_BT}\right) + \tanh\left(\frac{\hbar(\omega + \omega_g)}{2k_BT}\right)\right], \tag{21}$$

where A is a constant. Note that we have dropped the density-of-states factor, and that the argument of the tanh function is changed from $\hbar\omega/4k_BT$ to $\hbar\omega/2k_BT$. The quantity $2|\mu|$ has been replaced by ω_g, because the experimental gap frequency is at least an order of magnitude smaller than the expected chemical potential. The dashed lines in Figs. 9 and 10 are fits to the data, with $\hbar\omega_g = 9$ meV. The fit to the temperature dependence in Fig. 10 is surprisingly good. It has been shown elsewhere that the temperature dependence of χ'' measured for the $x = 0.5$, $T_c = 50$ K crystal is well described by the function $\tanh(\hbar\omega/2k_BT)$,[43] or, equivalently, $\tan^{-1}(\hbar\omega/k_BT)$.[44] (Similar scalings were first demonstrated for lightly doped La_2CuO_4.[26,45]) The comparison with the frequency dependence in Fig. 9 is less satisfactory but still quite good considering the simplicity of the formula. Certainly the model does not describe the peak at 30 meV observed at 10 K, and it misses the falloff at higher energies. [Of course, we have not included the optic-mode contribution to $\tilde{\chi}''(\omega)$, and that is likely to add weight at energies above 40 meV.] A calculation of the dynamical spin susceptibility based on the t-J model by Tanamoto, Kuboki, and Fukuyama[46] yields the same pseudogap in $\chi''(\mathbf{Q}_{\rm AF},\omega)$, but with a sharp peak immediately above the gap. In our data the gap and the peak are widely separated and do not appear to be directly related to one another. A more sophisticated model than Eq. (21) is required to describe these features.

The success in describing the temperature dependence of $\tilde{\chi}''(\omega)$ suggests that it might be applied to the relaxation rate measured for Cu in the CuO_2 planes by NMR. Figure 14 shows measurements of $(T_1T)^{-1}$ for Cu obtained by Takigawa *et al.*[47] in a sample with $x = 0.63$, $T_c = 60$ K. The quantity $(T_1T)^{-1}$ should be proportional to a weighted $\mathbf{Q}$ average of $\chi''(\mathbf{Q},\omega_0)$, where $\hbar\omega_0$ is orders of magnitude less than k_BT.[10] Assuming the dominant contribution to come from the region of $\mathbf{Q}_{\rm AF}$, we model the temperature dependence of $(T_1T)^{-1}$ with Eq. (21). The solid line in Fig. 14 is a rough fit to the data using $\hbar\omega_g = 18$ meV. The agreement is quite good.

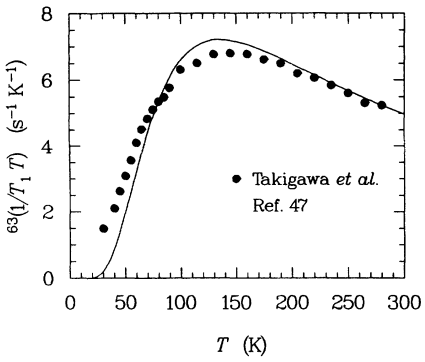

FIG. 14. Experimental results for $(T_1T)^{-1}$ for Cu in an $x = 0.63$ sample measured by Takigawa *et al.* (Ref. 47) (solid circles). The line is a fit to the data with Eq. (21) using $\hbar\omega_g = 18$ meV, as discussed in the text.

The motivation for modeling the relaxation-rate results was to check the consistency between the temperature dependence of χ'' observed in neutron scattering and NMR studies. The value of $\hbar\omega_g$ used to model $(T_1T)^{-1}$ for the $x = 0.63$ sample is twice that required by the neutron results for $x = 0.6$. Does this indicate a lack of consistency? Not necessarily, since it has been observed that the size of the low-temperature pseudogap varies rapidly with small changes in oxygen content.[16,17] Tanamoto, Kuboki, and Fukuyama[46] have pointed out that the rapid variation might be understandable if the size of the gap is proportional to the chemical potential. However, to rationalize such a picture, we still have to explain why the gap appears for the full Q width of the peak in χ'' and not just at $\mathbf{Q}_{\rm AF}$.

One possibility is that the structure we observe with neutrons is not that which is directly calculated in the Lindhard susceptibility but instead is entirely due to the effects of antiferromagnetic exchange interactions, as may appear in the random phase approximation. This scenario is very close to the result obtained by Si *et al.*[39] In their calculation of the Lindhard susceptibility, based on a tight-binding fit to band-structure calculations for $YBa_2Cu_3O_7$, a broad minimum is observed in the neighborhood of $\mathbf{Q}_{\rm AF}$. A strong peak in that region, comparable to that observed by neutron scattering, is obtained only by applying the RPA with a large, $\mathbf{Q}$-dependent exchange interaction. While they have not detected the spin gap in their analysis, a hint of it appears in their calculation of the temperature dependence of $\chi''(\mathbf{Q}_{\rm AF},\omega)$ at $\hbar\omega = 8$ meV. (It would be of interest to know the value of μ, and to see calculations at lower energies.) On the other hand, Si *et al.*[39] do find that, as a function of frequency, $\chi''(\mathbf{Q}_{\rm AF},\omega)$ peaks near 25 meV at low temperature, and that the peak amplitude decreases rapidly with temperature. They attribute this feature to a van Hove singularity in the density of states.

As emphasized by Zha *et al.*,[48] the source of the structure in the dynamic susceptibility is quite different in $YBa_2Cu_3O_{6+x}$ and $La_{2-x}Sr_xCuO_4$. Calculations[39,49] of the Lindhard susceptibility for the latter compound using a physically realistic Fermi surface directly yield the incommensurate structure that has been observed experimentally.[24,23] Thus, for that system the RPA correction is not necessary in order to obtain the correct $\mathbf{Q}$ dependence, so that the relevance of antiferromagnetic exchange interactions is more difficult to judge. In contrast, for $YBa_2Cu_3O_{6+x}$ the existence of a peak at $\mathbf{Q}_{\rm AF}$ cannot be explained as a simple Fermi-surface effect if one relies on the band structure obtained in density functional calculations.[50] Alternatively, a reasonable description of the $\mathbf{Q}$ and ω dependence of the susceptibility for $YBa_2Cu_3O_{6+x}$ can be obtained using a nested Fermi surface very close to half filling;[40] however, one must then explain why the chemical potential is pinned so close to zero.

D. Superconductivity

In the discussion above, we treated the temperature dependence of the measured dynamical susceptibility as if it was entirely due to normal-state properties of the CuO_2 planes, even though our measurements span the superconducting transition temperature. Let us now consider how the superconducting state, and especially the existence of an energy gap for Cooper pairs, might be expected to affect our results.

For our $x = 0.6$ crystal with $T_c = 53$ K, the BCS gap energy, $2\Delta = 3.5k_BT_c$, corresponds to 16 meV. This energy is indicated in Fig. 9. If the spectral weight at $\mathbf{Q}_{\rm AF}$ is due to the linear response of a Fermi liquid, calculations[37] for both s-wave and simple d-wave pairing indicate that the superconducting energy gap should show up in the dynamic spin susceptibility. In contrast, we clearly observe strong magnetic scattering well below the weak-coupling gap energy. Maleyev[51] has recently suggested that spin fluctuations might cause pair breaking, in which case the gap could be significantly reduced. To test that possibility, we need an independent measurement of the gap energy in $YBa_2Cu_3O_{6+x}$ for $x < 1$; however, we are not aware that any such data presently exist.

A simple way to explain the nonappearance of a superconducting gap in χ'' near $\mathbf{Q}_{\rm AF}$ would be the occurrence of microscopic electronic phase separation. Emery, Kivelson, and Lin[52] have pointed out that phase separation is observed in certain parameter regimes of various model Hamiltonians intended to approximate the behavior of CuO_2 planes. If the doped holes cluster in hole-rich regions, then the magnetic scattering from hole-poor regions would dominate the signal near $\mathbf{Q}_{\rm AF}$. If the hole-poor regions stay normal when the hole-rich regions go superconducting, then the energy gap would not appear in our measurements. As long as the normal regions have a characteristic size of a few lattice spacings, our data is consistent with such a picture. Unfortunately, the phase-separation model has not yet provided any positive predictions for the spin susceptibility.

V. SUMMARY

In this paper, we have presented a detailed study of the dynamical spin susceptibility in a single crystal of $YBa_2Cu_3O_{6.6}$ using inelastic neutron scattering. The imaginary part of the susceptibility at a fixed frequency is characterized by a broad peak centered about the wave vector for 2D antiferromagnetic ordering within a CuO_2 plane. It is also dependent on momentum transfers perpendicular to the layers due to a strong antiferromagnetic spin correlation between nearest-neighbor planes. As a function of frequency, $\chi''(\mathbf{Q}_{AF},\omega)$ peaks near 27 meV at a temperature of 10 K, with the amplitude in the region of the peak decreasing rapidly with increasing temperature.

A careful look at the shape of the susceptibility peak at $\mathbf{Q}_{AF}$ reveals that it is much more flat-topped and steep-sided than can be described by a single Gaussian function. A preliminary check of the 2D structure of the peak suggests that it is not isotropic about $\mathbf{Q}_{AF}$; instead, the data are consistent with a square shape, where the corners point along the [100] and [010] directions. Taking into account the rapid falloff of the peak away from the central plateau, the spectral weight seems sufficiently localized to explain the contrast in nuclear relaxation rates for Cu and O observed by NMR and NQR.

In contrast to the behavior at 9 meV and above, the spectral weight at 5 meV drops toward zero at temperatures below 50 K. We have shown that this gaplike behavior, together with the monotonic variations at higher energies, can be described rather well by a simple functional form adapted, with some pragmatic license, from a formula suggested by Bulut and Scalapino.[37] The formula involves a temperature-independent energy gap, which suggests that the observed low-temperature pseudogap is not directly related to the superconductivity. Even if it were, we observe significant spectral weight at energies well below the weak coupling estimate for 2Δ.

While our results may answer some questions, they raise others. Experiments are in progress to clarify further the temperature and $\mathbf{Q}$ dependence of χ'' in the $x = 0.6$ crystal, and also in crystals with higher oxygen content. Nevertheless, we hope that the present results will stimulate further theoretical analysis.

ACKNOWLEDGMENTS

Discussions with V. J. Emery have provided invaluable guidance throughout the course of this work. We also acknowledge stimulating conversations with R. J. Birgeneau. This study was supported by the U.S.-Japan collaborative Program on Neutron Scattering. Work at the Brookhaven National Laboratory was carried out under Contract No. DE-AC02-76CH00016, Division of Materials Sciences, U.S. Department of Energy.

APPENDIX A: ANALYTIC DECONVOLUTION

The resolution function has a Gaussian dependence on the deviations of momentum and energy transfer from their nominal values. If $S(\mathbf{Q},\omega)$ also has a Gaussian form, then the convolution with the resolution function can be performed analytically. To describe this process, we first consider the relevant coordinate systems and define some notation. The sample is oriented with [110] and [001] axes in the horizontal scattering plane; [1$\bar{1}$0] is vertical. Let Q_H, Q_K, and Q_z be the components of $\mathbf{Q}$ along [110], [001], and [1$\bar{1}$0], respectively. We will assume that the energy and Q_K dependences of the scattering function vary sufficiently slowly that we can pull them out of the convolution integral. Then we can write the scattering function defined by Eqs. (4) and (6) as

$$S(\mathbf{Q},\omega) = S_0(Q_K,\omega) \times \exp\{-[(Q_H - Q_H^c)^2 + (Q_z - Q_z^c)^2]/2\sigma^2\}, \tag{A1}$$

where, for a commensurate cross section, $Q_H^c = \sqrt{2}\pi/a$ and $Q_z^c = 0$. We assume that the width σ, which might vary with ω, is essentially constant within the resolution volume.

To describe the resolution function, it is convenient to introduce the four-vector $\mathcal{Q}$ such that

$$\mathcal{Q} = (\mathcal{Q}_0, \mathcal{Q}_1, \mathcal{Q}_2, \mathcal{Q}_3) \equiv \left(\frac{m_N}{\hbar Q}\omega, \mathbf{Q}\right). \tag{A2}$$

The resolution function is defined relative to the nominal values ω_0 and $\mathbf{Q}_0$ determined by the spectrometer setting. The elements of an arbitrary vector $\mathbf{Q}$ are specified as the in-plane projections parallel and perpendicular to $\mathbf{Q}_0$, labeled $Q_\parallel$ and $Q_\perp$, and the vertical component Q_z. Thus, $\mathcal{Q}_1 = Q_\parallel$, $\mathcal{Q}_2 = Q_\perp$, and $\mathcal{Q}_3 = Q_z$. Setting $\Delta\mathcal{Q} = \mathcal{Q} - \mathcal{Q}_0$, the resolution function can be written as

$$R(\mathcal{Q} - \mathcal{Q}_0) = R_0 \exp\left(-\tfrac{1}{2}\Delta\mathcal{Q}\cdot\mathsf{M}\cdot\Delta\mathcal{Q}\right). \tag{A3}$$

Analytic formulas for the elements of the resolution matrix M in terms of the incident and scattered neutron wave vectors and collimator divergences have been given by Cooper and Nathans[53] (note that we have transposed some rows of the resolution matrix relative to their definitions); the normalization factor is discussed by Chesser and Axe.[54] The measured intensity is given by

$$I = \left(\frac{\hbar Q_0}{m_N}\right)\int d^4\mathcal{Q}\, R(\mathcal{Q} - \mathcal{Q}_0)\, S(\mathcal{Q}). \tag{A4}$$

To perform the convolution integral, we must first transform the crystal coordinates Q_H and Q_K to spectrometer coordinates $Q_\parallel$ and $Q_\perp$. The required transformation is

$$Q_H = Q_\parallel \cos\theta - Q_\perp \sin\theta, \tag{A5}$$

$$Q_K = Q_\parallel \sin\theta + Q_\perp \cos\theta, \tag{A6}$$

where

$$\tan\theta = Q_K^0/Q_H^0. \tag{A7}$$

One can then combine Eqs. (A1), (A3), and (A4), and perform the integrals. The result is

$$I = P_0 S_0 \exp\left\{-\tfrac{1}{2}\left[\left(\frac{Q_H - Q_H^c}{\sigma_H}\right)^2 + \left(\frac{Q_z - Q_z^c}{\sigma_z}\right)^2\right]\right\}. \tag{A8}$$

The widths σ_H and σ_z are given by

$$\frac{1}{\sigma_H^2} = \frac{M'_{11}(A\sigma^2 + B) - (M'_{11}\sin\theta + M'_{12}\cos\theta)^2}{(M'_{11}\sigma^2 + \cos^2\theta)(A\sigma^2 + B)} \tag{A9}$$

and

$$\frac{1}{\sigma_z^2} = \frac{M_{33}}{1 + M_{33}\sigma^2}, \tag{A10}$$

where

$$A = M'_{11}M'_{22} - M'^2_{12}, \tag{A11}$$

$$B = M'_{11}\sin^2\theta + M'_{22}\cos^2\theta + 2M'_{12}\sin\theta\cos\theta, \tag{A12}$$

and

$$M'_{ij} = M_{ij} - (M_{0i}M_{0j}/M_{00}). \tag{A13}$$

The prefactor P_0 is given by

$$P_0 = \frac{(2\pi\sigma)^2(\hbar Q_0/m_N)R_0}{[M_{00}(A\sigma^2 + B)(1 + M_{33}\sigma^2)]^{1/2}}. \tag{A14}$$

To measure the width σ, we scan Q_H through Q_H^c at fixed Q_K with $Q_z = 0$. The observed width σ_H is a function of Q_K/Q_H, but we will ignore this variation and take $\tan\theta = Q_K/Q_H^c$. Thus, we expect to observe an approximately Gaussian peak with width σ_H. To obtain σ from σ_H, we solve Eq. (A9) using the calculated elements of the resolution matrix. The scattering function prefactor S_0 is determined from the fitted amplitude by dividing out the factor P_0 described by Eq. (A14).

As an aside, it may be helpful to explain the focusing effect observed in Fig. 3. The ellipsoid defined by the resolution matrix has an oblong shape. For a spectrometer having identical monochromator and analyzer crystals, and symmetric collimations with respect to the sample, the longest axis of the resolution ellipsoid lies in the ω-$Q_\perp$ plane when $\omega_0 = 0$. The commonly discussed form of focusing[53] involves aligning the slope of the ellipsoid in the ω-$Q_\perp$ plane with the dispersion surface being measured. Such a technique can greatly enhance measurements of transverse-acoustic phonons, but is of no use for studying magnetic scattering in metallic $YBa_2Cu_3O_{6+x}$. However, there is another feature of the resolution function that we can use to our advantage. At finite ω, the long axis of the ellipsoid rotates in the $Q_\perp$-$Q_\parallel$ plane, so that it is no longer purely transverse to $\mathbf{Q}_0$. As a result, as we scan along the rod $(\frac{1}{2}, \frac{1}{2}, l)$ at fixed ω, the long axis of the resolution ellipsoid will become parallel to the rod at some finite value of l. Scanning across the rod at the focused position yields the narrowest effective resolution width and an enhanced intensity. Note that this focusing effect is not symmetric in l; it occurs on only one side of $l = 0$.

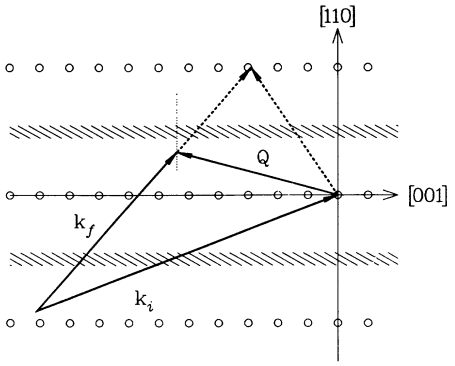

FIG. 15. Scattering diagram corresponding to the spurious peak observed in the 40 meV scan of Fig. 2. Solid lines indicate intended scattering process; dashed lines illustrate the accidental Bragg scattering condition.

APPENDIX B: ACCIDENTAL BRAGG SCATTERING

The explanation of spurious peaks due to accidental Bragg scattering was given by Currat and Axe.[55] It is fairly simple. At some point in an inelastic scan, the rotation angle of the sample crystal may become such as to allow Bragg diffraction. The analyzer setting will not allow detection of neutrons Bragg diffracted by the sample with the energy of the incident beam; however, any weak scattering process at the analyzer, such as inelastic scattering by phonons, may allow some of the spurious neutrons to reach the detector. Because Bragg scattering by the sample can be many orders of magnitude greater than the inelastic process of interest, weak scattering at the analyzer can result in a spurious peak comparable to or greater than the desired signal.

A diagram of the scattering condition for the spurious peak in the 40 meV scan of Fig. 2 is given in Fig. 15. As shown, the artifact occurs when the sample orientation corresponds to elastic scattering at $\mathbf{Q} = (1, 1, -2.9)$. The tail of the Bragg peak at $(1, 1, -3)$ is sufficient to cause a significant spurious signal. All of the observed spurious peaks correspond to $(1, 1, l)$ elastic scattering by the crystal. In some cases where we checked, there was no significant Bragg scattering of neutrons with the nominal incident energy. However, on removing the PG filter and going to two-axis mode, we found very strong scattering, presumably due to second-order neutrons. The presence of second-order neutrons in the incident beam greatly increases the chance of accidental Bragg scattering.

[1]P. A. Lee, in *The Los Alamos Symposium–1989: High Temperature Superconductivity*, edited by K. S. Bedell, D. Coffey, D. E. Meltzer, D. Pines, and J. R. Schrieffer (Addison-Wesley, Redwood City, CA, 1990), pp. 96–116.
[2]R. J. Birgeneau and G. Shirane, in *Physical Properties of High Temperature Superconductors*, edited by D. M. Ginsberg (World Scientific, Singapore, 1989), pp. 151–211.
[3]R. J. Cava, Science **247**, 656 (1990).
[4]J. M. Tranquada, in *Earlier and Recent Aspects of Superconductivity*, edited by J. G. Bednorz and K. A. Müller (Springer, Berlin, 1990), pp. 422–440.
[5]J. Rossat-Mignod, P. Burlet, M. J. Jurgens, C. Vettier, L. P. Regnault, J. Y. Henry, C. Ayache, L. Forro, H. Noel, M. Potel, P. Gougeon, and J. C. Levet, J. Phys. (Paris) **49**, C8-2119 (1988).
[6]J. M. Tranquada, A. H. Moudden, A. I. G. P. Zolliker, D. E. Cox, G. Shirane, S. K. Sinha, D. Vaknin, D. C. Johnston, M. S. Alvarez, A. J. Jacobson, J. T. Lewandowski, and J. M. Newsam, Phys. Rev. B **38**, 2477 (1988).
[7]G. Shirane, J. Als-Nielsen, M. Nielsen, J. M. Tranquada, H. Chou, S. Shamoto, and M. Sato, Phys. Rev. B **41**, 6547 (1990).
[8]J. M. Tranquada, W. J. L. Buyers, H. Chou, T. E. Mason, M. Sato, S. Shamoto, and G. Shirane, Phys. Rev. Lett. **64**, 800 (1990).
[9]J. Rossat-Mignod, L. P. Regnault, M. J. Jurgens, C. Vettier, P. Burlet, J. Y. Henry, and G. Lapertot, Physica B **163**, 4 (1990).
[10]R. E. Walstedt and W. W. Warren, Jr., Science **248**, 1082 (1990).
[11]A. J. Millis, in *The Los Alamos Symposium–1989: High Temperature Superconductivity* (Ref. 1), pp. 198–224.
[12]A. J. Millis, H. Monien, and D. Pines, Phys. Rev. B **42**, 167 (1990).
[13]H. Monien, D. Pines, and M. Takigawa, Phys. Rev. B **43**, 258 (1991).
[14]H. Chou, J. M. Tranquada, G. Shirane, T. E. Mason, W. J. L. Buyers, S. Shamoto, and M. Sato, Phys. Rev. B **43**, 5554 (1991).
[15]P. Bourges, P. M. Gehring, B. Hennion, A. H. Moudden, J. M. Tranquada, G. Shirane, S. Shamoto, and M. Sato, Phys. Rev. B **43**, 8690 (1991).
[16]P. M. Gehring, J. M. Tranquada, G. Shirane, J. R. D. Copley, R. W. Erwin, M. Sato, and S. Shamoto, Phys. Rev. B **44**, 2811 (1991).
[17]J. Rossat-Mignod, L. P. Regnault, C. Vettier, P. Burlet, J. Y. Henry, and G. Lapertot, Physica B **169**, 58 (1991).
[18]J. Rossat-Mignod, L. P. Regnault, C. Vettier, P. Bourges, P. Burlet, J. Bossy, J. Y. Henry, and G. Lapertot, Physica C **185-189**, 86 (1991).
[19]J. Rossat-Mignod, L. P. Regnault, C. Vettier, P. Bourges, P. Burlet, J. Bossy, J. Y. Henry, and G. Lapertot, in *Proceedings of the International Conference on Neutron Scattering, Oxford, 1991* [Physica B (to be published)].
[20]M. Sato, S. Shamoto, J. M. Tranquada, G. Shirane, and B. Keimer, Phys. Rev. B **61**, 1317 (1988).
[21]J. M. Tranquada, G. Shirane, B. Keimer, S. Shamoto, and M. Sato, Phys. Rev. B **40**, 4503 (1989).
[22]T. R. Thurston, R. J. Birgeneau, M. A. Kastner, N. W. Preyer, G. Shirane, Y. Fujii, K. Yamada, Y. Endoh, K. Kakurai, M. Matsuda, Y. Hidaka, and T. Murakami, Phys. Rev. B **40**, 4585 (1989).
[23]G. Shirane, R. J. Birgeneau, Y. Endoh, P. Gehring, M. A. Kastner, K. Kitazawa, H. Kojima, I. Tanaka, T. R. Thurston, and K. Yamada, Phys. Rev. Lett. **63**, 330 (1989).
[24]S. Cheong, G. Aeppli, T. E. Mason, H. Mook, S. M. Hayden, P. C. Canfield, Z. Fisk, K. N. Clausen, and J. L. Martinez, Phys. Rev. Lett. **67**, 1791 (1991).
[25]S. Shamoto, S. Hosoya, and M. Sato, Solid State Commun. **66**, 195 (1988).
[26]S. M. Hayden, G. Aeppli, H. Mook, D. Rytz, M. F. Hundley, and Z. Fisk, Phys. Rev. Lett. **66**, 821 (1991).
[27]R. J. Cava, A. W. Hewat, E. A. Hewat, B. Batlogg, M. Marezio, K. M. Rabe, J. J. Krajewski, J. W. F. Peck, and J. L. W. Rupp, Physica C **419**, 419 (1990).
[28]J. D. Jorgensen, B. W. Veal, A. P. Paulikas, L. J. Nowicki, G. W. Crabtree, H. Claus, and W. K. Kwok, Phys. Rev. B **41**, 1863 (1990).
[29]W. Reichardt, N. Pyka, L. Pintschovius, B. Hennion, and G. Collin, Physica C **162-164**, 464 (1989).
[30]W. Kress, U. Schröder, J. Prade, A. D. Kulkarni, and F. W. de Wette, Phys. Rev. B **38**, 2906 (1988).
[31]S. L. Chaplot, Phys. Rev. B **37**, 7435 (1988).
[32]Y. J. Uemura *et al.*, Phys. Rev. Lett. **62**, 2317 (1989).
[33]A. Bianconi, P. Castrucci, M. Pompa, A. M. Flank, P. Lagarde, H. Katayama-Yoshida, and G. Calestani, in *Earlier and Recent Aspects of Superconductivity*, edited by J. G. Bednorz and K. A. Müller (Springer, Berlin, 1990), pp. 407–421.
[34]H. Ehrenreich and M. H. Cohen, Phys. Rev. **115**, 786 (1959).
[35]J. P. Rice, J. Giapintzakis, D. M. Ginsberg, and J. M. Mochel, Phys. Rev. B **44**, 10 158 (1991).
[36]N. Bulut, D. Hone, D. J. Scalapino, and N. E. Bickers, Phys. Rev. Lett. **64**, 2723 (1990).
[37]N. Bulut and D. J. Scalapino (unpublished).
[38]J. P. Lu, Q. Si, J. H. Kim, and K. Levin, Physica C **179**, 191 (1991).
[39]Q. Si, Y. Zha, K. Levin, J. P. Lu, and J. H. Kim (unpublished).
[40]J. Ruvalds, C. T. Rieck, J. Zhang, and A. Virosztek, Science **256**, 1664 (1992).
[41]A. Virosztek and J. Ruvalds, Phys. Rev. B **42**, 4064 (1990).
[42]C. M. Varma, P. B. Littlewood, S. Schmitt-Rink, E. Abrahams, and A. E. Ruckenstein, Phys. Rev. Lett. **63**, 1996 (1989).
[43]J. M. Tranquada, in *High-Temperature Superconductivity: Physical Properties, Microscopic Theory, and Mechanisms*, edited by J. Ashkenazi, S. E. Barnes, F. Zuo, G. C. Vezzoli, and B. M. Klein (Plenum, New York, 1991), p. 629.
[44]R. J. Birgeneau, R. W. Erwin, P. M. Gehring, M. A. Kastner, B. Keimer, M. Sato, S. Shamoto, G. Shirane, and J. Tranquada, Z. Phys. B **87**, 15 (1992).
[45]B. Keimer, R. J. Birgeneau, A. Cassanho, Y. Endoh, R. W. Erwin, M. A. Kastner, and G. Shirane, Phys. Rev. Lett. **67**, 1930 (1991).
[46]T. Tanamoto, K. Kuboki, and H. Fukuyama, J. Phys. Soc. Jpn. **60**, 3072 (1991).
[47]M. Takigawa, A. P. Reyes, P. C. Hammel, J. D. Thompson, R. H. Heffner, Z. Fisk, and K. C. Ott, Phys. Rev. B **43**, 247 (1991).
[48]Y. Zha, Q. Si, K. Levin, and J. P. Lu (unpublished).
[49]P. B. Littlewood, J. Zaanen, G. Aeppli, and M. Monien (unpublished).
[50]W. E. Pickett, H. Krakauer, R. E. Cohen, and D. J. Singh,

Science **255**, 46 (1992).
[51]S. V. Maleyev (unpublished).
[52]V. J. Emery, S. A. Kivelson, and H. Q. Lin, Phys. Rev. Lett. **64**, 475 (1990).
[53]M. J. Cooper and R. Nathans, Acta Crystallogr. **23**, 357 (1967).
[54]N. J. Chesser and J. D. Axe, Acta Crystallogr. A **29**, 160 (1973).
[55]R. Currat and J. D. Axe (unpublished).